Analytical Methods

www.rsc.org/methods

Volume 4 | Number 8 | August 2012 | Pages 2191–2586

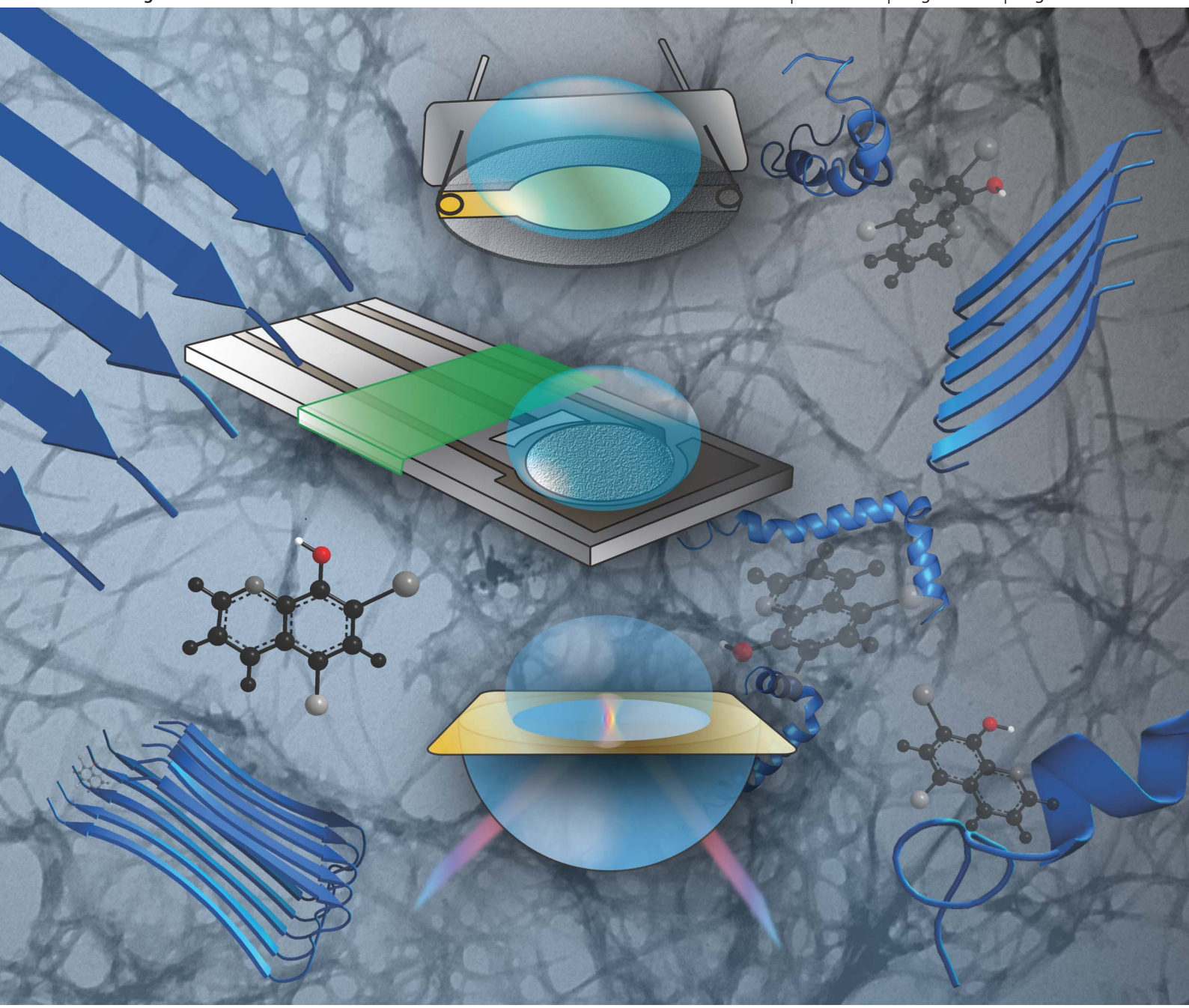

ISSN 1759-9660

RSC Publishing

PAPER

Kerman *et al.*

Label-free methods for probing the interaction of clioquinol with amyloid-β

Analytical Methods

Dynamic Article Links

Cite this: *Anal. Methods*, 2012, **4**, 2228

www.rsc.org/methods

PAPER

Label-free methods for probing the interaction of clioquinol with amyloid-β†

Xin Ran Cheng,[a] Vinci Wing Sze Hung,[a] Simona Scarano,[b] Marco Mascini,[b] Maria Minunni*[b] and Kagan Kerman*[a]

Received 4th February 2012, Accepted 5th May 2012
DOI: 10.1039/c2ay25123j

The presence of amyloid-β (Aβ) fibrils is characteristic of Alzheimer's disease (AD), and the aggregation of these amyloidogenic proteins is a nucleation-dependent process. In this report, label-free methods based on surface plasmon resonance (SPR) and thickness shear mode acoustic wave sensors (TSM-AWS) were used to detect monomer elongation in real-time. The modulation of Aβ aggregation using a well-described flavonoid, clioquinol (CQ) was also observed. Established methods like fluorescence and electrochemistry were also employed to confirm the interaction of CQ with Aβ. Good correlation between the designed label-free methods creates a promising platform for the screening of novel amyloid inhibitors.

Introduction

Alzheimer's disease (AD) is a neurodegenerative disease marked by clinical symptoms such as a decline in cognitive ability, alterations in behaviour, irreversible memory loss, and language impairment.[1] The onset of the disease is not considered a natural pathway of aging[2] and is the most prevalent cause of dementia with about 18 to 30 million patients worldwide.[3] AD is one of the most common neurodegenerative diseases including Parkinson's, Huntington's, and Creutzfeld Jacob disease, in which symptom progression is correlated to the development of neural fibrillary tangles and neuritic plaques deposited within the limbic and association cortices of the brain.[4,5] One of the major neuropathological hallmarks of AD is the deposition of amyloid-β (Aβ) on the walls of cerebral and meningeal blood vessels as senile plaques. Amyloid is the generic term describing abnormally fibrillated proteins possessing a β-pleated sheet conformation. In AD, the central core of senile plagues comprise insoluble amass of fibrillated aggregates of Aβ. The cytotoxic effect of these conformers had been correlated to the onset and progression of permanent cognitive impairments to memory, learning, and language.[6] Aβ1-42 in AD patients are formed when amyloid precursor protein gets cleaved by β- and γ-secretases to produce Aβ1-40 and Aβ1-42.[7] Recently, it has been reported that the oligomeric forms of Aβ are neurotoxic.[8] There is also accumulating evidence that monomeric form of Aβ seems to mediate the growth of AD amyloid plaques in human brain rather than mature fibrils.[9] Therefore, the study of monomer elongation might provide clues to therapeutic interventions.

Aggregation of Aβ is a nucleation-dependent process.[10] Nucleation is followed by the accelerated aggregate growth and incorporation of soluble aggregates (intermediate species) before forming mature fibrillar networks. Several advanced analytical techniques such as circular dichroism spectroscopy, high-resolution atomic force microscopy and nuclear magnetic resonance have been applied to study the mechanisms of amyloid formation.[11] However, most of these techniques require complex instrumentation and tedious sample preparation steps. As such, robust and rapid analytical methods are greatly desired to develop multiplexed platforms for AD drug screening nowadays, considering the recent aging population crisis in developed countries.

Recently, reports have been published about the applications of surface plasmon resonance (SPR) and piezoelectric sensors to monitor Aβ aggregation.[12–22] Buell and co-workers[12] studied the interactions between organic dyes and Aβ on a thickness shear mode acoustic wave sensor (TSM-AWS). They proposed that TSM-AWS could elucidate the interaction of potential inhibitors with Aβ.[12] Yamada and co-workers[15–18] used SPR to characterize the effect of Aβ concentration on aggregation, and calculated the critical monomer concentration as 20 nM and equilibrium binding constant of monomers to fibrils as 5×10^7 M^{-1}. Alkaloids have been tested using SPR to observe their effects on Aβ aggregation.[15–18] TSM-AWS studies have proposed a "dock and lock" mechanism to describe rapid binding of monomers to fibril aggregates occurring rapidly in a reversible fashion, which was then followed by a conformational change in structure that stabilized the aggregates.[22] The stabilization process generated new binding sites to allow further docking of new monomers to the aggregates.[22]

Clioquinol (CQ, 5-chloro-7-iodo-8-hydroxyquinoline) was reported to significantly reduce Aβ plaque deposits, and improve

[a]*Department of Physical and Environmental Sciences, University of Toronto Scarborough, Toronto, ON, M1C 1A4, Canada. E-mail: kagan.kerman@utoronto.ca; Fax: +1 416 287 7279; Tel: +1 416 287 7279*
[b]*Dipartimento di Chimica "Ugo Schiff", Università degli Studi di Firenze, Via della Lastruccia 3, 50019 Sesto Fiorentino, Italy. E-mail: maria.minunni@unifi.it; Fax: +39 055 457 3384; Tel: +39 055 457 3314*
† Electronic supplementary information (ESI) available: Additional supporting figures and table. See DOI: 10.1039/c2ay25123j

cognitive behaviour in humans.[23,24] It was shown that oral administration of CQ significantly hindered Aβ accumulation in the brain of Tg2576 mice, and in clinical studies, patients exhibited slower cognitive decline after CQ treatment.[23,24]

In this study, label-free biosensing methods were developed to evaluate the Aβ1-42 aggregation in real-time, starting from seeds immobilized on the sensing surface to act as initiators. This system was also used to test the inhibitory activity of CQ on Aβ1-42 aggregation. The results of the label-free methods were supported using the electrochemical and fluorescence data.

Experimental

Materials and instruments

Amyloid-β (Aβ) peptide Aβ1-42 trifluoroacetic salt was purchased from EMD Chemicals Inc. (Gibbstown, NJ) (peptide sequence: DAEFRHDSGYEVHHQKLVFFAEDVGSNK-GAIIG LMVGGVVIA). Thioflavin T (ThT, 4-(3,6-dimethyl-1,3-benzothiazol-3-ium-2-yl)-*N*,*N*-dimethylaniline chloride), multi-walled carbon nanotubes (MWCNT, 110–170 nm in diameter, 5–9 μm in length, 90+% purity), graphite powder (<20 μm, synthetic), mineral oil, ammonium iron(II)sulfate hexahydrate, ethanolamine HCl (EA), clioquinol (CQ), zinc(II) chloride, 11-mercapto-1-undecanoic acid (MUA), 1-ethyl-3-(3-dimethyl-aminopropyl) carbodiimide (EDC) and copper(II) chloride were purchased from Sigma Aldrich (Oakville, ON). *N*-Hydroxysuccinimide (NHS) was purchased from Fluka (Milan, Italy). All solutions were prepared using double-distilled MilliQ water, unless otherwise stated. Ammonia (28%) was purchased from VWR. Hydrogen peroxide (35%) was obtained from Merck (Germany). Ethanol and all the reagents for the buffers were purchased from Merck (Italy).

For SPR measurements, the running buffer contained 5 mM *N*-2-hydroxyethylpiperazine-*N*′-2-ethanesulfonic acid (HEPES, pH 7.4), 5 mM HEPES–Na with 150 mM NaCl, 3 mM EDTA and 0.005% surfactant P20. The buffer was filtered and degassed before use. EDTA was purchased from Merck (Milan, Italy). Immobilization buffer contained 10 mM acetic acid and 10 mM sodium acetate (trihydrate) before adjusting pH using NaOH to pH 5. Phosphate Buffer Saline (PBS, 50 mM, pH 7.4) with 100 mM NaCl was also used. All other chemicals were of analytical grade and used without further purification.

Quartz crystals (9.5 MHz AT-Cut, 14 mm) with gold evaporated (42.6 mm^2 area) onto both sides were purchased from International Crystal Manufacturing (Oklahoma, USA). The measurements were conducted in methacrylate cells, where only one side of the crystal was in contact with the solution. The quartz crystal analyzer used for the measurements was the Model QCA922 (Seiko EG&G, Chiba, Japan) for TSM-AWS studies. The frequency shifts were calculated from the difference between two stable frequency signals (±1 Hz).

For SPR measurements, the Biacore X™ (Biacore AB Uppsala, Sweden) was used with the research grade Au chip (SIA kit Au). Thermomixer Comfort (Eppendorf, Hamburg, Germany) was used for the incubation of fibrils. The change in resonance units (RU) was recorded in real time on a sensorgram where 1 RU was equivalent to one picogram per square millimeter on the sensor surface.

Label-free methods: TSM-AWS and SPR

Aβ1-42 peptides were dissolved in DMSO and stored at −20 °C. The monomers were obtained from the stock solution by sonicating the peptides for 5 min before storing at −20 °C until use. The peptides were also diluted to 40 μM using PBS, and then subjected to 24 h incubation at 37 °C with shaking at 800 rpm in order to produce the fibril seeds.

All fibril seeds and monomers were sonicated for at least 5 min before use in attempts to obtain the seed solution. Cleaning of the quartz crystal was performed by boiling for 10 min in a 5 : 1 : 1 (v/v) mixture of water : ammonia : hydrogen peroxide, respectively. The crystal was then incubated in 95% ethanol for 1 h before immersing in 1 mM MUA overnight to allow film formation. The immobilization chemistry involved the covalent peptide bond forming process. The activation of the carboxylic groups was achieved by reacting the MUA-modified surface with an aqueous solution of 5.8 mg mL^{-1} NHS and 38.3 mg mL^{-1} EDC for 15 min. The fibril seeds were diluted in PBS to 15 μM, and sonicated. An aliquot (100 μL) of fibril seeds was introduced to the activated MUA surface for 30 min. The fibril seed-immobilized surface was then rinsed with PBS to remove non-specifically bound species before adding 1 M EA for 15 min to block any remaining active esters on the surface. An aliquot (100 μL) of 2 μM Aβ1-42 peptide monomers in the absence and presence of 10 μM CQ was then exposed to the seed-immobilized surface for 50 min before a subsequent PBS wash. The change in frequency signals before and after monomer incubation was recorded.

For SPR measurements, the surface cleaning and modification procedures were adapted from the detailed study of Mariotti *et al.*[25] For the EDC/NHS activation of the MUA-modified surface, the solution was flown at 5 μL min^{-1} for 7 min followed by the addition of fibril seeds for 30 min at a flow rate of 3 μL min^{-1}. In order to quench the active esters, EA was also added for 10 min at 5 μL min^{-1}. The monomer and CQ were injected at a flow rate of 2 μL min^{-1} for 50 min. The flow rates were adapted from the detailed study of Mariotti *et al.*[25] The change in RU before and after monomer incubation was recorded.

Sample preparation for electrochemistry and fluorescence

Solutions were prepared in PBS with 100 mM NaCl and stored at 4 °C until use. ThT stock solutions (10 mM) were prepared fresh with ultrapure water, and stored at room temperature while shielded from light to prevent photodegradation. A working solution of 250 μL was prepared containing 50 μM of Aβ1-42 in the presence and absence of 50 μM CQ incubated at 37 °C with shaking to induce the aggregation of Aβ1-42.

Preparation of multi-walled carbon nanotube-modified carbon paste electrode (CNT-CPE)

Composition of the CNT-CPE consisted of 10% MWCNT, 60% graphite powder and 30% mineral oil by weight. Constituents were mixed thoroughly until a thick paste was created. The paste was then packed into a carbon paste working electrode body with 3.0 mm internal diameter. Surface of the CNT-CPEs were smoothed between experiments on a weighing paper.

Square wave voltammetry (SWV)

The working electrode was pre-treated each time before a measurement for 60 s at 1.7 V in PBS, then rinsed with ultrapure water. An aliquot (15 μL) of sample was placed on an inverted CNT-CPE and allowed to adsorb for a duration of 15 min at room temperature. A final rinsing step was done for 5 s using 10 mL of PBS. Measurements were taken in 10 mL of solution of PBS using SWV with a potential range from 0 to 1.3 V at a frequency of 230 Hz.

Fluorescence spectroscopy

Aβ1-42 and CQ samples were prepared in 50 mM PBS with 100 mM NaCl at pH 7.4. ThT fluorescence was collected at 440 nm excitation and 485 nm emission. All samples were incubated at 37 °C with shaking. The experimental results were analyzed using Gen5 Microplate Data Collection and Analysis Software.

Results and discussion

For an effective monitoring of Aβ1-42 elongation, it was crucial to avoid non-specific adsorption of Aβ1-42 monomers on the biosensor surface. With this objective in mind, MUA film was first formed on the quartz crystal surface and then activated with EDC/NHS chemistry. The surface was directly saturated with EA in the absence of seeds, to obtain a 'control'. On the EA-passivated surface, a 2 μM monomer solution of Aβ1-42 and subsequently, a 10 μM CQ solution were tested, both showing negligible signals (Fig. S1A and B†). This result showed that the non-specific adsorption of the monomers and CQ on the surface could be suppressed by applying EA.

Aβ1-42 sample was incubated for 24 h at 37 °C to form mature fibrils (Fig. S2A†). The fibrils were then sonicated to disintegrate into small fragments (coined here as 'seeds') (Fig. S2B†). The seeds were then immobilized on the covalently activated surface. The surface was then blocked with EA, so that the unreacted esters

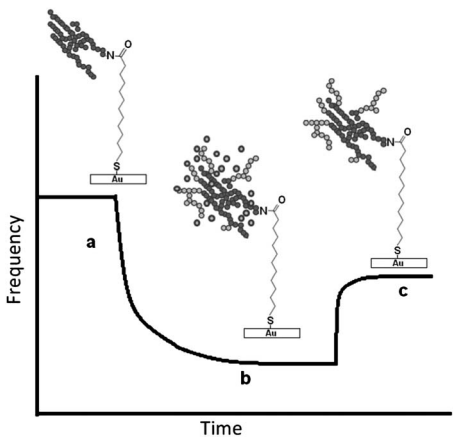

Fig. 1 Fibril elongation process on the surface of the seed-immobilized TSM-AWS; (a) baseline signal in buffer, before Aβ1-42 monomer addition on the seed-immobilized surface; (b) deposition and elongation of Aβ1-42 fibrils; (c) surface wash to remove the non-specifically bound monomers. The analytical signal was calculated as the difference (c–a) in frequency (Hz).

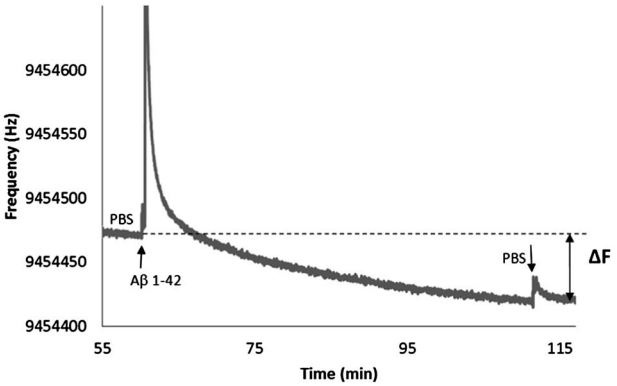

Fig. 2 Frequency (Hz) *vs.* time (min) plot showing the decrease in net frequency change (Δ*F*) after a 50 min incubation of 2 μM Aβ1-42 monomers on the seed-immobilized surface.

would not create further binding sites during the addition of monomers (Fig. 1). The serial introduction of 2 μM Aβ1-42 monomers on the seed-immobilized surface for 50 min induced a decrease in the measured frequency of 46 ± 7 Hz (Table S1† and Fig. 2). The net decrease in frequency is correlated to the mass increase on the TSM-AWS. This result supported the previous hypothesis that fibril formation initiated from nuclei sites.[27–37] Bini *et al.*[38] estimated that the mass deposited for a change of 1 Hz would correspond to 20 pg mm^{-2}. From our data, the mass change was about 15 Hz, and thus corresponded to 300 pg mm^{-2} of seeds immobilized on the surface. When 10 μM CQ was simultaneously introduced with 2 μM monomer solution for 50 min, the net decrease in frequency became 6.0 Hz, which was significantly smaller than the monomer incubation on its own. During the serial injections, the presence of CQ with monomers induced a net increase in frequency (Fig. 3). This implied that the freshly elongated immobilized seeds were lifting off from the sensor surface. In order to show that the small change in frequency was not due to the saturation of the seed-immobilized surface, an incubation of 2 μM monomer solution alone was performed with the surface for 50 min, and the net decrease in frequency was 41 Hz. This recovery of the drop in frequency indicated that CQ inhibited the elongation by interacting more with monomers, but less with the fibril seeds on the surface.

CQ alone was also introduced to a seed-immobilized surface, but the net change in frequency (Fig. S3†) was negligible

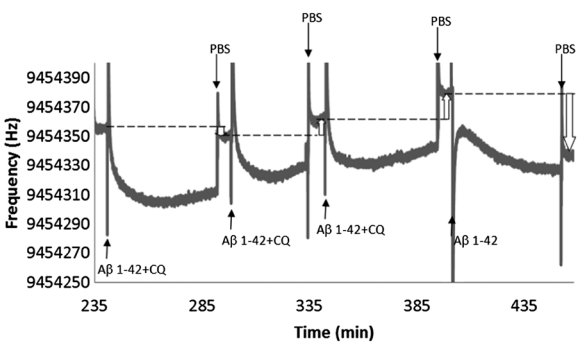

Fig. 3 Serial injections of 2 μM Aβ1-42 monomers with 10 μM CQ. Subsequent injections of 2 μM Aβ1-42 monomers initiated the elongation process.

indicating that CQ had a weak affinity to the immobilized seeds on the surface. This was attributed to the hydrophilicity of the halogen and hydroxyl groups on CQ that prevented the interaction of CQ with the hydrophobic core of the fibrils. The results of these control measurements are listed in Table S1†.

For SPR measurements, the immobilization chemistry and elongation procedures were similar to that described for the TSM-AWS-based method. SPR sensorgrams showed different characteristics of binding to the surface in both cases (Fig. S4A and B†). Preliminary assays were carried out to verify the suppression of non-specific adsorption. When Aβ1-42 monomers in the presence and absence of CQ were introduced to the passivated gold surface, RU signals of about 162 ± 22 and 276 ± 20 were observed, respectively (Fig. S5†). The monomers in the presence of CQ resulted in a consistently smaller RU increase than in its absence. When 2 μM Aβ1-42 monomers were introduced to the seed-immobilized surface, a significant response of 541 ± 61 RU was observed, which indicated the attachment of monomers on the seed-immobilized surface. CQ was also introduced to the EA-passivated surface to test for its non-specific adsorption on the surface, but only a negligible signal was observed (data not shown).

To ensure that the Aβ1-42 was 'growing' on the sensor surface, four subsequent control experiments were also performed (Fig. S6†). The results obtained showed stepwise increase in RU after each injection of the monomers. An increase of approximately 2000 RU was observed after all the injections, which corresponded to 32 ng of Aβ1-42 being deposited on the surface with a channel of 16 mm^2 area (1000 RU = 1 ng mm^{-2}).[39]

To increase the SPR signal for fibril elongation, the concentration of seeds was doubled to 30 μM. According to Cannon and co-workers,[26] the increase in seed concentration would result in an increase in the elongation rate. Our results were in consensus with those previously reported values, as the RU increase was almost doubled in a time span of 50 min.

Injection of monomers in the presence of 10 μM CQ, caused an almost 5-fold decrease in RU. CQ alone was also introduced to the seed-immobilized surface, and did not cause a significant change in the signal (Fig. 4).

To confirm the results obtained from the label-free studies of Aβ1-42 aggregation *in vitro*, electrochemical and fluorescence measurements were performed. Electrochemical monitoring of Aβ aggregation was performed using the well-established oxidation peak of a lone tyrosine residue (Tyr-10) intrinsic to

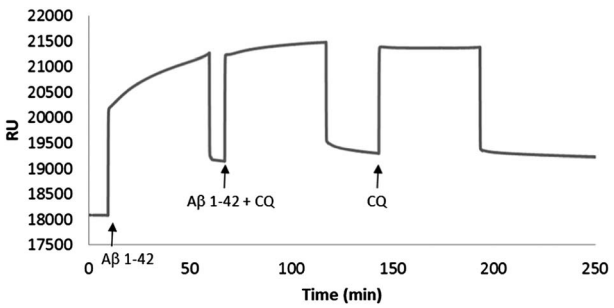

Fig. 4 Sensorgram showing the inhibitory effect of 10 μM CQ on aggregation, when introduced in the presence and absence of 2 μM Aβ1-42 on the seed-immobilized surface.

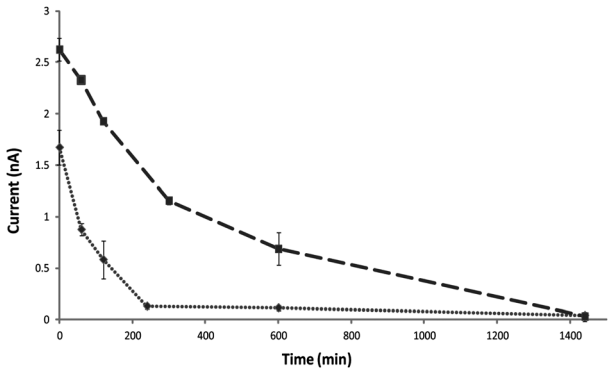

Fig. 5 The dependence of Tyr-10 oxidation signal of Aβ1-42 on time in the absence (dotted line) and presence of 50 μM CQ (dashed line). Error bars represent the standard deviation of triplicate measurements ($n = 3$).

human Aβ1-42.[40,41] The magnitude of the oxidation signal at approximately 0.7 V (*vs.* Ag/AgCl) was recorded over a 24 h time span. As Aβ1-42 peptides aggregated, and formed large, ordered, fibrillar species, Tyr-10 became more shielded within the peptide, therefore less available to be oxidized at the electrode surface. This caused the observed oxidation signal to decrease as the aggregation continued.

It was expected that in the absence of aggregation modulators, Aβ1-42 alone would show the most rapid decrease in Tyr-10 oxidation signal, while after the addition of CQ, the time required to reach the same extent of aggregation would increase.

As shown in Fig. 5, electrochemical assessment of Aβ1-42 aggregation kinetics supported this hypothesis, as the decrease was most significant for the incubation with Aβ1-42 alone, and plateaued shortly after 200 min passed. A similar phenomenon has been reported recently,[42] when baicalein was incubated with α-synuclein, another amyloidogenic protein, and thus, confirmed the validity of our electrochemical analysis.

In the presence of CQ, the decrease in the oxidation signal of Tyr-10 progressed slowly. This indicated that the aggregation of Aβ1-42 was modulated by the flavonoid. As well, the overall current intensity recorded for Aβ1-42 in the presence of CQ was

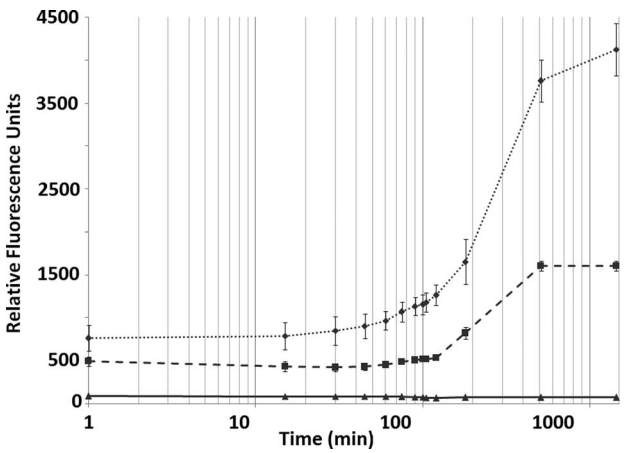

Fig. 6 The dependence of ThT fluorescence signal on time with 50 μM Aβ1-42 in the absence (dotted line) and presence (dashed line) of 50 μM CQ. Solid line demonstrates that 50 μM CQ alone did not show significant fluorescence activity. Error bars represent the standard deviation of triplicate measurements ($n = 3$).

higher than that of Aβ1-42 alone, suggesting that the aggregates formed in the presence of CQ were less densely packed, and as such allowed for more Tyr-10 residues to be oxidized.

A similar trend was observed in our fluorescence analysis as depicted in Fig. 6. The use of ThT as a fluorescent dye to monitor β-sheet formation during peptide aggregation was described extensively in the past, and as such, provided a reliable method to validate the results obtained from our label-free experiments. In the absence of CQ, Aβ1-42 alone showed the most significant increase in fluorescence intensity, as well as the highest values of relative fluorescence unit (RFU), as expected. Fluorescence of CQ alone was also monitored to make sure that there were no significant RFU contributions that could complicate the values recorded for Aβ1-42 in the presence of CQ.

Upon addition of CQ, the first notable difference was the slower rate of increase in fluorescence. The final intensity of ThT fluorescence in the presence of CQ was also less intense as compared to that in its absence. These results corresponded to what had been observed in the previously described label-free methods in this report, further supporting the ability of CQ to modulate the progression of Aβ1-42 aggregation.

Conclusions

The modulation effects of CQ were observed on the aggregation of Aβ1-42 peptides using piezoelectric and SPR-based methods. The design of these label-free methods shows good promise in rapid and cost-effective screening for aggregation modulators, which would be highly valuable in developing new therapeutic agents against AD. High-throughput, multiplexed label-free analysis of novel aggregation modulators is under investigation in our laboratory.

Acknowledgements

This work was financially supported by the Alzheimer Society of Canada and NSERC Discovery Grant.

Notes and references

1 R. E. Tanzi, *Nat. Neurosci.*, 2005, **8**, 977–979.
2 A. Rauk, *Chem. Soc. Rev.*, 2009, **38**, 2698–2715.
3 T. L. Kukar, T. B. Ladd, M. A. Bann, P. C. Fraering, R. Narlawar, G. M. Maharvi, B. Healy, R. Chapman, A. T. Welzel, R. W. Price, B. Moore, V. Rangachari, B. Cusack, J. Eriksen, K. Jansen-West, C. Verbeeck, D. Yager, C. Eckman, W. Ye, S. Sagi, B. A. Cottrell, J. Torpey, T. L. Rosenberry, A. Fauq, M. S. Wolfe, B. Schmidt, D. M. Walsh, E. H. Koo and T. E. Golde, *Nature*, 2008, **453**, 925–929.
4 G. G. Glenner, C. W. Wong, V. Quaranta and E. D. Eanes, *Appl. Pathol.*, 1984, **2**, 357–369.
5 K. A. Jellinger, *Acta Neuropathol.*, 2009, **118**, 1–3.
6 R. Shapira, G. E. Austin and S. S. Mirra, *J. Neurochem.*, 1988, **50**, 69–74.
7 M. Citron, D. Westaway, W. Xia, G. Carlson, T. Diehl, G. Levesque, K. Johnson-Wood, M. Lee, P. Seubert, A. Davis, D. Kholodenko, R. Motter, R. Sherrington, B. Perry, H. Yao, R. Strome, I. Lieberburg, J. Rommens, S. Kim, D. Schenk, P. Fraser, P. St George Hyslop and D. J. Selkoe, *Nat. Med.*, 1997, **3**, 67–72.
8 B. A. Yankner, L. R. Dawes, S. Fisher, L. Villa-Komaroff, M. L. Oster-Granite and R. L. Neve, *Science*, 1989, **245**, 417–420.
9 B. P. Tseng, W. P. Esler, C. B. Clish, E. R. Stimson, J. R. Ghilardi, H. V. Vinters, P. W. Mantyh, J. P. Lee and J. E. Maggio, *Biochemistry*, 1999, **38**, 10424–10431.
10 J. D. Harper and P. T. Lansbury Jr, *Annu. Rev. Biochem.*, 1997, **66**, 385–407.
11 M. Bartolini, M. Naldi, J. Fiori, F. Valle, F. Biscarini, D. V. Nicolau and V. Andrisano, *Anal. Biochem.*, 2011, **414**, 215–225.
12 A. K. Buell, E. K. Esbjörner, P. J. Riss, D. A. White, F. I. Aigbirhio, G. Toth, M. E. Welland, C. M. Dobson and T. P. J. Knowles, *Phys. Chem. Chem. Phys.*, 2011, **13**, 20044–20052.
13 S. A. Kozin, Y. V. Mezentsev, A. A. Kulikova, M. I. Indeykina, A. V. Golovin, A. S. Ivanov, P. O. Tsvetkov and A. A. Makarov, *Mol. BioSyst.*, 2011, **7**, 1053–1055.
14 Q. Wang, N. Shah, J. Zhao, C. Wang, C. Zhao, L. Liu, L. Li, F. Zhou and J. Zheng, *Phys. Chem. Chem. Phys.*, 2011, **13**, 15200–15210.
15 K. Hasegawa, K. Ono, M. Yamada and H. Naiki, *Biochemistry*, 2002, **41**, 13489–13498.
16 K. Ono, Y. Yoshiike, A. Takashima, K. Hasegawa, H. Naiki and M. Yamada, *J. Neurochem.*, 2003, **87**, 172–181.
17 K. Ono, K. Hasegawa, H. Naiki and M. Yamada, *Biochim. Biophys. Acta, Gen. Subj.*, 2004, **1690**, 193–202.
18 M. Hiohata, K. Hasegawa, S. Tsutsumi-Yasuhara, Y. Ohhashi, T. Ookoshi, K. Ono, M. Yamada and H. Naiki, *Biochemistry*, 2007, **46**, 1888–1899.
19 B. Bohrmann, M. Adrian, J. Dubochet, P. Kuner, F. Müller, W. Huber, C. Nordstedt and H. Döbeli, *J. Struct. Biol.*, 2000, **130**, 232–246.
20 B. Bohrmann, L. Tjernberg, P. Kuner, S. Poli, B. Levet-Trafit, J. Näslund, G. Richards, W. Huber, H. Döbeli and C. Nordstedt, *J. Biol. Chem.*, 1999, **274**, 15990–15995.
21 B. E. Kraziński, J. Radecki and H. Radecka, *Sensors*, 2011, **11**, 4030–4042.
22 J. A. Kotarek, K. C. Johnson and M. A. Moss, *Anal. Biochem.*, 2008, **378**, 15–24.
23 C. W. Ritchie, A. I. Bush, A. Mackinnon, S. Macfarlane, M. Mastwyk, L. MacGregor, L. Kiers, R. Cherny, Q.-X. Li, A. Tammer, D. Carrington, C. Mavros, I. Volitakis, M. Xilinas, D. Ames, S. Davis, K. Beyreuther, R. E. Tanzi and C. L. Masters, *Arch. Neurol.*, 2003, **60**, 1685–1691.
24 R. A. Cherny, C. S. Atwood, M. E. Xilinas, D. N. Gray, W. D. Jones, C. A. McLean, K. J. Barnham, I. Volitakis, F. W. Fraser, Y. Kim, X. Huang, L. E. Goldstein, R. D. Moir, J. T. Lim, K. Beyreuther, H. Zheng, R. E. Tanzi, C. L. Masters and A. I. Bush, *Neuron*, 2001, **30**, 665–676.
25 E. Mariotti, M. Minunni and M. Mascini, *Anal. Chim. Acta*, 2002, **453**, 165–172.
26 M. J. Cannon, A. D. Williams, R. Wetzel and D. G. Myszka, *Anal. Biochem.*, 2004, **328**, 67–75.
27 L. Cahoon, *Nat. Med.*, 2009, **15**, 356–359.
28 P. Schuck, *Annu. Rev. Biophys. Biomol. Struct.*, 1997, **26**, 541–566.
29 J. Ryu, H.-A. Joung, M.-G. Kim and B. P. Chan, *Anal. Chem.*, 2008, **80**, 2400–2407.
30 C. D. Syme, R. C. Nadal, S. E. J. Rigby and J. H. Viles, *J. Biol. Chem.*, 2004, **279**, 18169–18177.
31 V. A. Streltsov, S. J. Titmuss, V. C. Epa, K. J. Barnham, C. L. Masters and J. N. Varghese, *Biophys. J.*, 2008, **95**, 3447–3456.
32 A. Lomakin, D. B. Teplow, D. A. Kirschner and G. B. Benedeki, *Proc. Natl. Acad. Sci. U. S. A.*, 1997, **94**, 7942–7947.
33 Y. Fezoui and D. B. Teplow, *J. Biol. Chem.*, 2002, **277**, 36948.
34 M. R. Nichols, M. A. Moss, D. K. Reed, W. L. Lin, R. Mukhopadhyay, J. H. Hoh and T. L. Rosenberry, *Biochemistry*, 2002, **41**, 6115–6127.
35 M. M. Pallitto and R. M. Murphy, *Biophys. J.*, 2001, **81**, 1805–1822.
36 J. Bieschke, J. Russ, R. P. Friedrich, D. E. Ehrnhoefer, H. Wobst, K. Neugebauer and E. E. Wanker, *Proc. Natl. Acad. Sci. U. S. A.*, 2010, **107**, 7710–7715.
37 H. LeVine III, Q. Ding, J. A. Walker, R. S. Voss and C. E. Augelli-Szafran, *Neurosci. Lett.*, 2009, **465**, 99–103.
38 A. Bini, M. Minunni, S. Tombelli, S. Centi and M. Mascini, *Anal. Chem.*, 2007, **79**, 3016–3019.
39 M. Abrantes, M. T. Magona, L. F. Boyd and P. Schuck, *Anal. Chem.*, 2001, **73**, 2828–2835.
40 M. Vestergaard, K. Kerman, M. Saito, N. Nagatani, Y. Takamura and E. Tamiya, *J. Am. Chem. Soc.*, 2005, **127**, 11892–11893.
41 M. Vestergaard and K. Kerman, *Curr. Pharm. Anal.*, 2009, **5**, 229–245.
42 T. Chan, A. M. Chow, D. W. F. Tang, Q. Li, X. Wang, I. R. Brown and K. Kerman, *J. Electroanal. Chem.*, 2010, **648**, 151–155.

